Dalton Transactions

Accepted Manuscript

ROYAL SOCIETY OF CHEMISTRY

www.rsc.org/dalton

A simple but efficient strategy to enhance hydrostability of intensely fluorescent Mg–based coordination polymer (CP) via forming composite of CP with hydrophobic PVDF

Lu Zhai, [a, b] Wen–Wei Zhang,*[a] Jing–Lin Zuo,[a] Xiao–Ming Ren*[b]

[a] *State Key Laboratory of Coordination Chemistry, School of Chemistry and Chemical Engineering, Nanjing University, Nanjing 210093 P. R. China. E–mail: wwzhang@nju.edu.cn*

[b] *State Key Laboratory of Materials–Oriented Chemical Engineering and College of Chemistry & Molecular Engineering, Nanjing Tech University, Nanjing 210009, P. R. China. E–mail: xmren@njtech.edu.cn*

Abstract

A coordination polymer (CP) of Mg^{2+} with 1, 3, 5−benzenetricarboxylate (BTC^{3-}) was synthesized by use of solvothermal method. The Mg–CP, with a formula of $Mg_3(BTC)(HCOO)_3(DMF)_3$, crystallizes in the trigonal space group *P–3*, with cell parameters of $a = b = 13.972(5)$ Å, $c = 8.090(5)$ Å and $V = 1367.6(11)$ $Å^3$, and shows a lamella structure built from planar rosette–type hexanuclear architectures. The Mg–CP emits intense blue fluorescence arising from $\pi^* \rightarrow \pi$ transition of intra–ligand of BTC^{3-} with 21.69 % quantum yield, yet it exhibits poor stability to water. The composites of Mg–CP with hydrophobic polyvinylidenefluoride (PVDF) were sequentially prepared by mechanically mixed, tableted and annealed processes, which showed good compatibility between Mg–CP and PVDF, high hydrostability and intense blue emission. This study suggests a simple but efficient method to solve the drawbacks of some functional CPs unstable to water and to promote them practical applications in the field of functional materials.

Keywords: Coordination polymer; composite; hydrostability; fluorescence

Introduction

The construction of coordination polymers (CPs) or metal−organic framework (MOFs) is currently attracting considerable attention because of their potential applications in a wide range of areas including adsorption,[1] separation,[2] ion exchange,[3] catalysis,[4] magnetism,[5] optics,[6] proton conductor,[7] fluorescence sensor,[8] and dielectric property[9] as well as many other application fields.[10] Most of CPs/MOFs are built from main group, transition or rare earth metal ions with carboxylate bridging ligands, which frequently possess high thermostability, however, poor hydrostability (even atmospheric moisture levels) due to the weak acidity of carboxylic acid. This drawback restricts the practical applications of CPs/MOFs in many aspects.[11] To solve this issue, the developed strategy is that the hydrophobic functional ligand is designed for construction of the CPs/MOFs or the modifiable functional groups are preset in the carboxylate ligands and then the hydrophobic framework is achieved by post−synthesis method,[12] obviously, such methods result in the complexity of preparation process.

Up to date, the majority of CPs/MOFs are concerned with transition metal and rare earth metal ions,[13] the main group metal magnesium−based CPs/MOFs are relatively unexplored. Surely, the rare reported Mg−based CPs/MOFs is mainly because of the inherent difficulties concerning their formation and crystallization.[14] Besides this, another reason is maybe that most magnesium−based CPs/MOFs are quite moisture−sensitive, even under atmospheric conditions.[15]

In this study, we achieved a two−dimensional magnesium−based coordination polymer (Mg−CP) with a tricarboxylic acid, which emits blue fluorescence with quite high quantum yield of 21.69 % in the solid state at ambient temperature, but, shows poor stability to water. In order to enhance the hydrostability of such a fluorescence CP, we explored to form the composites of Mg−CP with the chemically resistant and hydrophobic polyvinylidenefluoride (PVDF). As anticipated, the intensely fluorescent composites show much higher stability to water. Herein, we present the synthesis, characterization and investigation of the fluorescence property for Mg−CP@PVDF composites.

Experimental Section

Reagents and materials

All reagents and materials are of analytical grade and used as received from commercial sources without further purification.

Physical measurements

The morphologies of the sample were obtained using a HITACHI–S4300 scanning electron microscope (SEM) and a Nikon DIA–PHOT 300 optical microscope. Thermal gravimetric analyses (TGA) were performed using a DTA–TGA 2960 thermogravimetric analyzer in nitrogen atmosphere with a heating rate of 10 °C/min from 30 to 800 °C. Thermo–gravimetric–mass spectrometric (TG–MS) analyses were performed in nitrogen atmosphere with a heating rate of 10 °C/min from 30 to 580 °C, using a NETZSCH STA449C instrument. Powder X–ray diffraction (PXRD) data and variable temperature powder X–ray diffraction (VT PXRD) data were recorded on a Bruker D8 Discover diffractometer with Cu Kα (λ = 1.54056 Å) radiation at a scan speed of 5 °/min and a step size of 0.02° in 2θ. The IR spectra were obtained on a NICOLET iS10 spectrometer in the 4000–400 cm^{-1} region. Photoluminescence spectra were recorded with a RF–5301PC spectrophotometer equipped with a 150 W Xenon lamp as an excitation source for in solid state sample at room temperature. PLQY and CIE 1931 color coordinates were measured using a Horiba Jobin Yvon FluoroMax–4 spectrofluorometer, equipped with an F–3018 integrating sphere.

Preparation of Mg–CP and composites

Synthesis of Mg–CP ($Mg_3(BTC)(HCOO)_3(DMF)_3$)**.** A mixture of 1, 3, 5–benzenetricarboxylic acid (10 mg, 0.048 mmol), $Mg(NO_3)_3\cdot 6H_2O$ (25 mg, 0.095 mmol), DMF (0.6 mL) and H_2O (0.10 mL) were stirred for ten minutes and then transferred to a 10 mL Teflon–lined autoclave and heated to 110 °C for 24 h.

Colorless block–shaped crystals of Mg–CP (hereinafter referred to as **1**) were achieved after slowly cooled to room temperature (yield: 75% based on Mg). Anal. Calcd for $C_7H_9MgNO_5$: C, 39.76; H, 4.26; N, 6.62. Found: C, 39.58; H, 4.31; N, 6.84. Selected IR data (KBr pellet, cm^{-1}): 3425 (w), 2973 (w), 2938 (w), 2883 (w), 1675 (w), 1640 (w), 1616 (w), 1502 (s), 1440 (w), 1389 (w), 1250 (s), 1108 (s), 948 (m), 867 (s), 781 (s), 719 (s).

Preparation of 1@PVDF composites. CP **1** was mixed with a certain amount of PVDF, and the mass percentage of **1** is 5, 10, 15, 20, 25 and 30% in each composite, respectively. As a representative, the preparation process of 5% **1**@PVDF composite is described in detail. Firstly, 5 mg powder of **1** was mixed with 95 mg PVDF, the mixtures were manually ground with the pestle to afford fine powder. Secondly, the mixtures were loaded into cylindrical punches and die with 13 mm diameters and then the powered samples were pressed into a pellet under the pressure of ca. 6 MPa with a thickness of ca. 0.30 mm. Finally, the 5% **1**@PVDF composite pellet was heated at 190 °C in an oven for 1 hour. The analogous procedure above–mentioned was used for preparation of other **1**@PVDF composites (Table S1).

Crystallographic data

Suitable single crystal of **1** was carefully selected under an optical microscope and glued to thin glass fibers. Single crystal X–ray diffraction data were collected on a Bruker Smart Apex II CCD diffractometer at 296 K using graphite monochromated Mo/Kα radiation (λ = 0.71073 Å). Data reductions and absorption corrections were performed with the SAINT[16] and SADABS2[17] software packages, respectively. Structures were solved by a direct method using the SHELXL–97 software package.[18] The non–hydrogen atoms were anisotropically refined using the full–matrix least–squares method on F^2. All hydrogen atoms were placed at the calculated positions and refined riding on the parent atoms. The crystallographic data and details of structural refinements for **1** are listed in Table 1 and selected bond distances and angles are listed in Table S2 in the Supporting Information, respectively.

Table 1 Crystallographic data and structural refinements for **1**

Compound	**1**
Formula	$C_7H_9MgNO_5$
Formula weight	211.46
CCDC no.	1061986
Temperature (K)	296(2)
Wavelength (Å)	0.71073
Crystal size /mm	0.30×0.25×0.18
Crystal system	Hexagonal
Space group	*P–3*
a / Å	13.972(5)
b / Å	13.972(5)
c / Å	8.090(5)
α/ (°)	90
β / (°)	90
γ/ (°)	120
V / Å^3	1367.6(11)
Z	6
$F(000)$	660
$\theta_{\mathrm{min,max}}$/°	0.945–24.990
GOF	1.027
$R_1{}^a$, $wR_2{}^b$ $[I > 2\sigma(I)]$	0.0303, 0.0754

$^aR_1=\sum||F_0|-|F_c|/\sum|F_0|$; $^bwR_2=\{\sum[w(F_0{}^2-F_c{}^2)^2]/\sum[w(F_0{}^2)^2]\}^{1/2}$

Results and Discussion

Crystal structure of 1. It is worth mentioning that the crystal structure of **1** was previously reported by others,[19] however, we obtain better photoluminescence property of **1** in our work. To better understand the relationship between its crystal structure and intense fluorescence, the crystal structure is simply described again. Single crystal X–ray analysis revealed that **1** crystallizes in the trigonal space group *P–3*. As shown in Fig. 1a, an asymmetric unit of **1** consists of one Mg^{2+} ion, one third of fully deprotonated BTC^{3-} ligand, one bridging $HCOO^-$ anion and one coordinated DMF molecule. The Mg1 ion is coordinated by six oxygen atoms with a slightly distorted octahedral geometry, where two oxygen atoms (O1 and O3) are from two carboxyl groups of BTC^{3-} ligands, three oxygen atom (O2, O2#3, O5) are from three carboxyl groups of $HCOO^-$ anions and the remaining one (O_4) is from DMF molecule

(Fig. 1b). Each BTC^{3-} in **1** binds to six Mg^{2+} ions via the oxygen atoms of carboxyl groups and adopts a hexadentate μ_6 coordination mode (Fig. 1c). The adjacent Mg^{2+} ions are connected together by two bridging formate ligands and two bidentate carboxylate oxygen atoms from the same BTC^{3-} ligand to form a novel hexanuclear Mg^{2+} cluster. Such Mg^{2+} cluster shows a 3–fold rotation symmetry (Fig. 2a) and served as secondary building units (SBUs). The SBUs are further linked together by six carboxylates to form planar rosette–type architecture (Fig. 2b). Analysis of the crystal packing of **1** reveals that such hexanuclear motifs stack along the [001] direction to display a layered appearance with distance of 8.090(5) Å, and six DMF molecules coordinate to six Mg^{2+} ions along the axial position of the planar hexanuclear SBU, three up and three down, which reside between two layers and fill in the void space, preventing the interpenetrating framework formation (Fig. 3a).

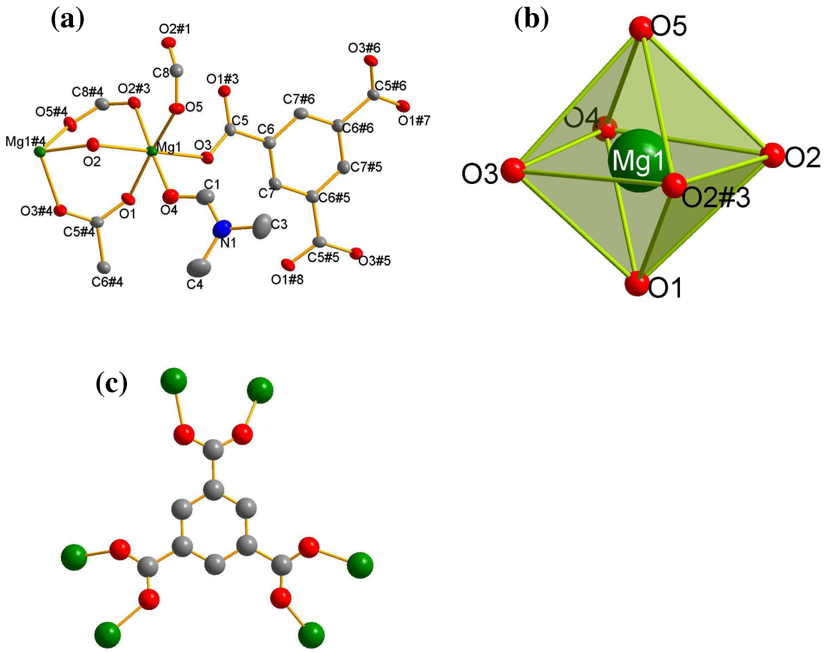

Fig. 1 (a) ORTEP plot of **1** showing the local coordination environment of Mg^{2+} with thermal ellipsoids at 50% probability; (b) the coordination polyhedron of the Mg^{2+} ion; (c) the coordination environment of BTC^{3-} (all H atoms were omitted for clarity and symmetry codes: #1 = –y, x–y, z; #2 = –x + y, –x, z; #3 = x–y, x, 1–z; #4 = y, –x + y, 1–z; #5 = 1–y, x–y, z; #6 = 1–x + y, 1–x, z; #7= 1 +y, 1–x+ y, 1–z; #8= 1 –x, – y, 1–z. Color scheme: C, gray; N, blue; O, red; Mg, green).

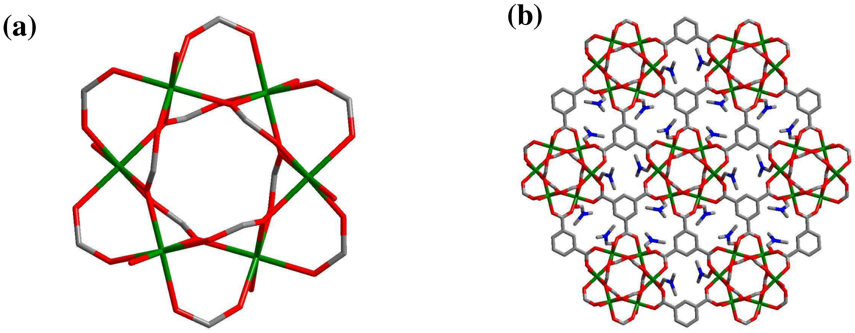

Fig. 2 (a) View of a hexanuclear Mg^{2+} cluster as SBU; (b) extended structure shown along [001]. All hydrogen atoms were omitted for clarity. Color scheme: C, gray; N, blue; O, red; Mg, green.

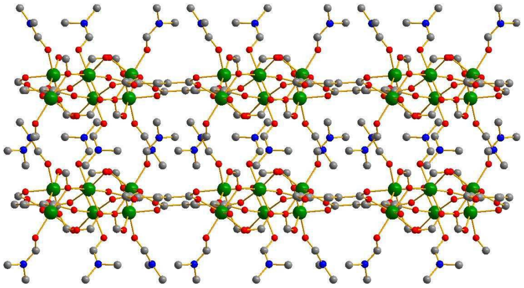

Fig. 3 Structures of **1** contain alternating layers in which DMF molecules lie between these layers along [001] direction.

TG and VT–PXRD of 1. The thermal and structural stabilities of **1** were measured by TG and VT–PXRD, which are displayed in Fig. 4 and Fig. 5 respectively. From the TG curve depicted in Fig. 4, the coordinated DMF molecules start to release at ca. 200 °C and this process is stabilized up to ca. 270 °C. The mass loss percentage of this stage is estimated to be ~21%, much less than the theoretical value of 34.5% corresponding to all DMF molecules completely removed from the interlayer spaces, revealing that ca. 40% DMF molecules are still remained between the interlayer spaces of **1** at ca. 270 °C. The remained coordinated DMF molecules can be removed around 420 °C according to the TG curve. As all DMF released, the interlayer space will be decreased.

The results of VT–PXRD measurements of **1** showed that the powder diffraction peaks disappeared till the temperature is over 420 °C, indicating the collapse of the framework structure after the removal of all coordinated DMF molecules, which is in accordance with the TG analysis. The most profound changes in reflection positions and intensities occurred in the temperature range up to 210 °C, during which the coordinated DMF molecules began to leave the structure according to the TG analysis. Actually, it is observed that the diffraction at 2θ = 10.95° related to (001) crystallographic plane splits into two peaks when the temperature is over 250 °C, and the new peak is located at higher angle side, indicating that the interlayer space is part decreased owing to DMF removal. The diffraction of (001) at 2θ = 10.95° still appears when the temperature is up to 400 °C, demonstrating the existence of part DMF molecules residual between the interlayer spaces at this temperature, which is further confirmed by TG–Mass measurement (ref. Fig. S1). Above 350 °C, the layered structure of **1** is destroyed accompanied by the loss of the remaining DMF molecules and the decomposition of $HCOO^{-}$ and BTC^{3-} ligands. It is well known that pure DMF is decomposed at its boiling point (151 °C), it is a quite rare case that it can be thermally stable to so high temperature (400 °C), which is due to DMF being confined between the interlayer spaces of **1**, and this is so–called ‘confined effect’.

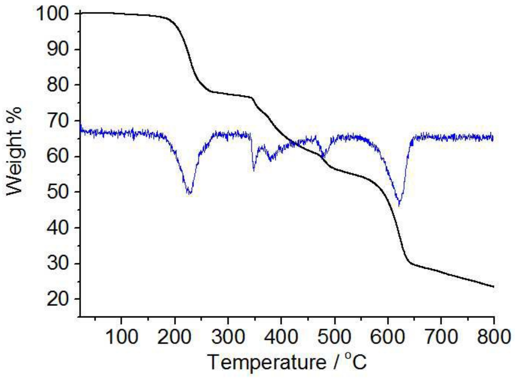

Fig. 4 TG and DTA plot of **1**.

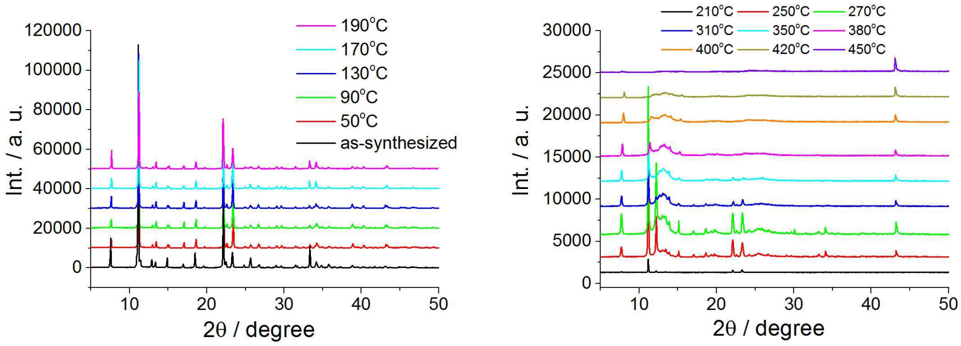

Fig. 5 VT–PXRD patterns for CP **1** in the temperature range of 50–450 °C.

Characterization of composites. Fig. 6a and 6b show the photos of two types of pellets for both neat PVDF and **1**@PVDF composite before and after annealed at 190 °C. All pellets are cylindrical with flat ends, with respect to the corresponding pellets before annealed at 190 °C, the annealed pellets exhibit good mechanical strength (i.e., hardness) and shrunken dimension. Fig. 6c–6e show the pellet morphologies of annealed neat PVDF and **1**@PVDF composite with 25wt% amount of **1**. It can be seen that crystals of **1** are well mixed and homogeneously distributed into the matrix of PVDF and no obvious aggregation was observed, and this behavior is probably attributed to the compatibility between DMF molecules of the crystal surface of **1** and PVDF. The IR spectra of PVDF and the composites with different CP amounts were recorded and are given in Figure S2 in the supplementary material. For PVDF, the strong band at 1211 cm^{-1} and 1181 cm^{-1} could be attributed to the stretching vibration of CF_2, and the bands at 874 and 1402 cm^{-1} were assigned to the C–C vibration and the deformation vibration of CH_2, respectively. As for the composites, the band arising from the characteristic stretching vibration of CF_2 (1181 cm^{-1}) were observed, suggesting the presence of PVDF phase in the composites. Moreover, the spectra of all composites exhibit similar bands corresponding to the symmetric and asymmetric vibrations of the carboxylate groups of the organic ligand (1603–1670 cm^{-1}), as well as its out of plane vibrations (below 1300 cm^{-1}). And the intensity of the characteristic C=O stretching vibration of is gradually increased as the amount of **1** is increased in the composites. All above further indicate that compound

1 is well mixed with the PVDF matrix.

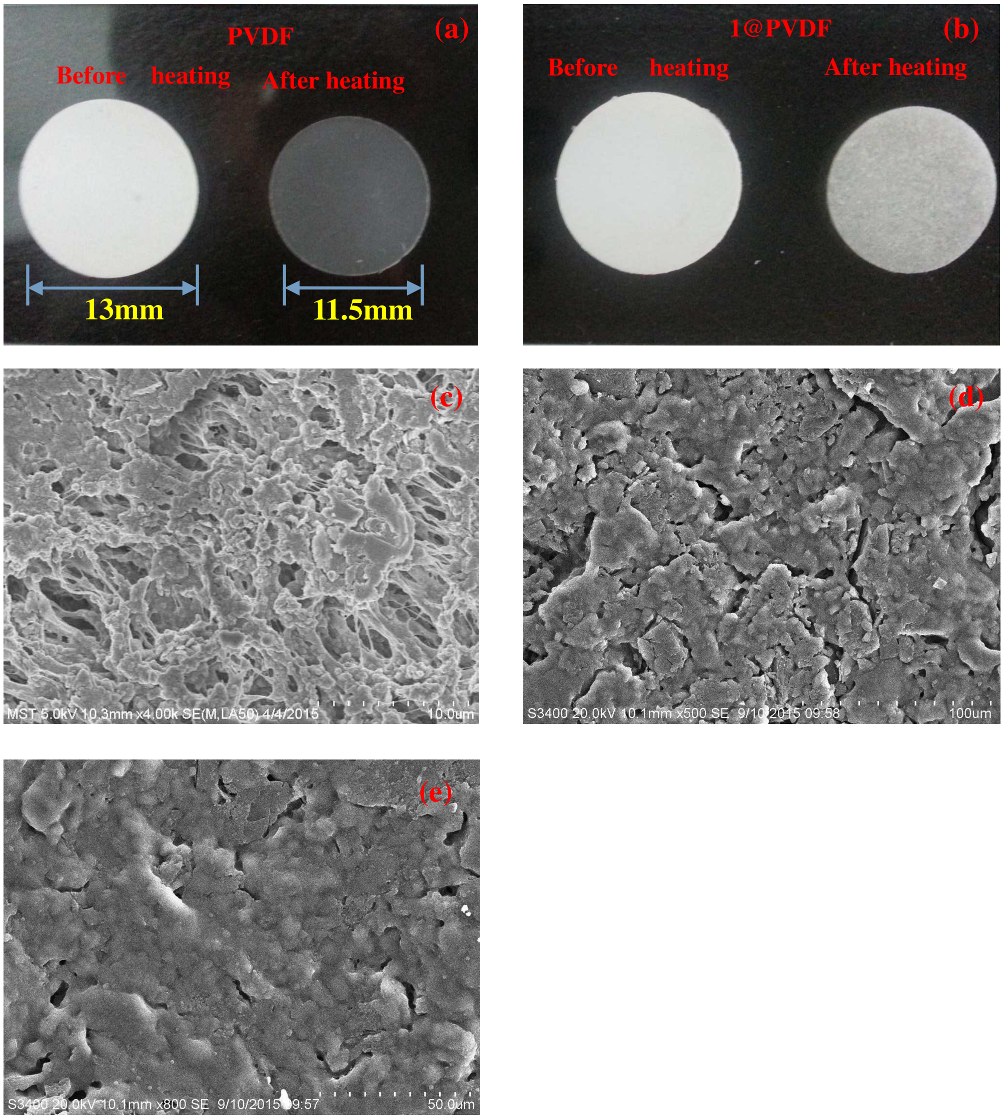

Fig. 6 Photos of (a) cylindrical pellets of neat PVDF and (b) 25 wt% **1**@PVDF composite before and after heating at 190 °C, and SEM images of annealed pellets of (c) PVDF and (d, e) 25 wt% **1**@PVDF composite under different magnifications.

PXRD profiles of annealed neat PVDF, before and after annealed **1**@PVDF composites at 190 °C are collected in Fig. 7. For neat PVDF, the well–defined diffraction peak at 2θ = ca. 18, 20° and 27°, respectively, are in agreement with the data published in the literature.[20] The characteristic diffraction peaks of **1** are visible when **1** is incorporated into PVDF matrix with amount of only 5%, and the characteristic diffractions intensity of **1** gradually increases with increasing the amount of **1** in the composites. By comparison of before and after annealed samples, the relative diffraction intensity of **1** become weakened in the composites annealed at 190 °C, demonstrating that the annealing process results in the reduction of crystallinity for **1**.

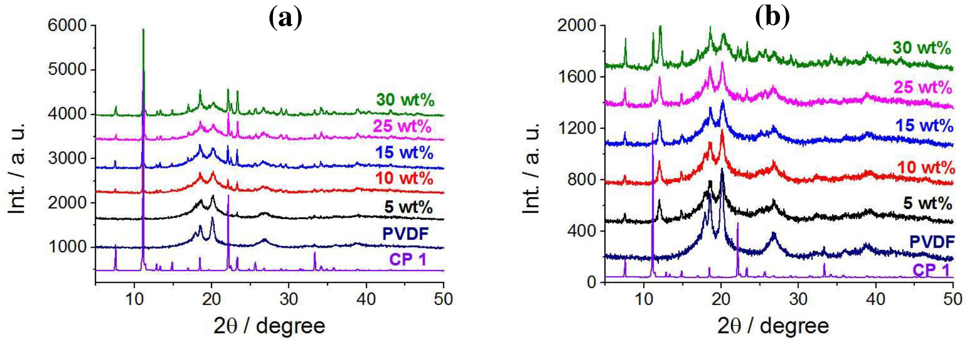

Fig. 7 PXRD patterns of **1**@PVDF: (a) before annealed; (b) after annealed at 190 °C.

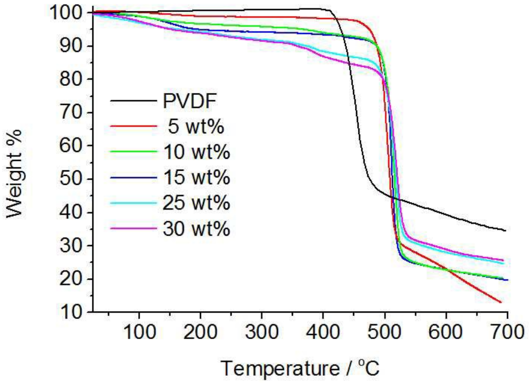

Fig. 8 TG curves of annealed neat PVDF and annealed **1**@PVDF composites.

The thermal stabilities of PVDF and **1**@PVDF composites are investigated by TGA. As displayed in Fig. 8, the onset temperature for releasing DMF is lower in each **1**@PVDF composite than that in **1**, which is probably related to the fact that the annealing process results in the reduction of crystallinity for **1**; while the critical temperature of residual DMF release in each **1**@PVDF composite sample is almost the same as that in **1**. Another worth mentioned point is that formation of composite enhances the thermostability of PVDF.

CP **1** is easily dissolved in water and unstable even in humid atmosphere, which is confirmed by PXRD analysis. As shown in Fig. S3, the PXRD pattern was completely changed when the as–prepared crystals of **1** were exposed in humid air for 2 days. As an example, we further investigated the hydrostability of 30 wt% **1**@PVDF composite before and after annealed at 190 °C. As shown in Fig. 9a, the characteristic diffractions arising from **1** disappear completely when the unannealed 30 wt% **1**@PVDF sample was exposed to atmosphere with a relative humidity of 55–75%, indicating that such a composite shows poor stability to moisture. However, as displayed in Fig. 9b, the annealed composite is more resistant to humidity at the same humidity atmosphere. In addition, the sample of unannealed 30 wt% **1**@PVDF composite was completely decomposed when it was immersed in water for 20 minutes, whereas the characteristic diffractions of **1** clearly appear in the PXRD profile of the annealed 30 wt%@PVDF composite even if it was immersed in water for four days (Fig. S4).

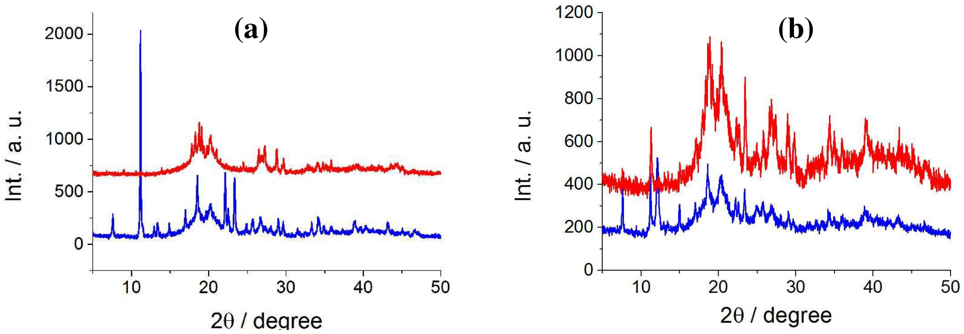

Fig. 9 PXRD patterns of two 30 wt% **1**@PVDF composite against humidity: (a) not annealed; (b) annealed at 190 °C. The blue and red lines represent before and after exposure to humid air for 10 days, respectively.

Photoluminescent properties

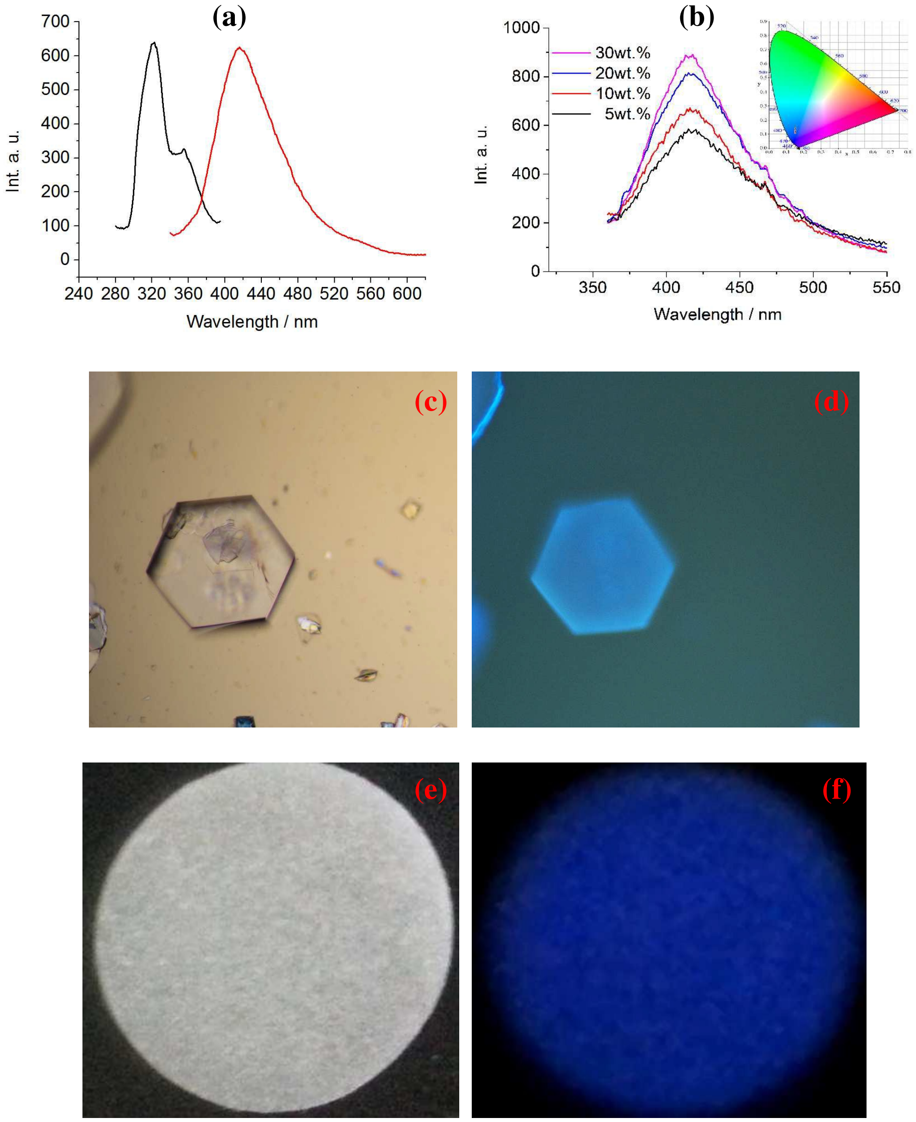

Fig. 10 (a) Excitation (black) and emission (red) spectra of **1** in the solid state at ambient temperature; (b) emission spectra of annealed **1**@PVDF composites (inset: the CIE coordinates of the composites); photos of crystal **1** under (c) ambient and (d) ultraviolet irradiation; photos of annealed 30 wt% **1**@PVDF composite pellet under (e) ambient and (b) ultraviolet irradiation.

The fluorescent spectra of **1** and H_3BTC in the solid state are recorded at room temperature using 322 nm light excitation. As shown in Fig. S5, H_3BTC showed a weak emission band centered at 380 nm, this emission band is attributed to the $\pi^* \rightarrow \pi$ transitions.[21] Contrast to the weak fluorescence of H_3BTC, CP **1** exhibits intense blue–purple light emission with a maximum around 415 nm at room temperature with CIE 1931chromaticity coordinate (0.16259, 0.1353) in the solid state (Fig. 10a and 10d). The emission band of **1** is similar to that of H_3BTC, but red–shifts 35 nm. The quantum yield reaches to 21.69 % for **1** at room temperature, which is much higher than other reported Mg–based CPs.[22] The excitation spectrum of **1** displays a main sharp peak centered at 322 nm with a weak discernible shoulder at 355 nm, which is related to the $\pi\rightarrow\pi^*$ transition within the BTC^{3-} ligand.[23] Usually, in the solid state, the excimers are easily formed between $\pi\cdots\pi$ stacking aromatic molecules, leading to the fluorescence quenching via intramolecular vibration relaxation, so the molecular crystal with strong $\pi\cdots\pi$ stacking interactions often shows weak $\pi\rightarrow\pi^*$ transition emission. The above crystal structure analysis disclosed that the BTC^{3-} ligands connect Mg^{2+} ions to form two–dimensional layer in **1**, but the neighboring layers are separated by the axial DMF ligands to prevent from the formation of $\pi\cdots\pi$ stacking, maybe this is the main reason why **1** shows such an intense emission.

The emission spectra of annealed **1**@PVDF composite pellets recorded at room temperature are shown in Fig. 10b. All spectra showed emission band around 415 nm which were in accordance with the emission band of **1**. The relative emission intensity of the composites gradually increases with increasing the amount of **1** in them. As anticipated, the composites maintained the intense fluorescence (Fig. 10f) which makes them potentially suitable for high efficient fluorescence materials in practical application.

Conclusion

In summary, we have achieved an intense blue emission Mg–based coordination polymer by solvothermal reaction, which is sensitive to water. The composite of Mg–based coordination polymer with hydrophobic PVDF was prepared using mechanically mixed and then annealed process, which tremendously improved its hydrostability. Moreover, the composites emit the characteristically intense fluorescence of Mg–based coordination polymer. This study suggests a simple but efficient approach to enhance the hydrostability of CPs/MOFs, which presents a new direction to promote CPs/MOFs−based functional materials for practical use.

Acknowledgments

Authors thank the Priority Academic Program Development of Jiangsu Higher Education Institutions, Special Research Found for the Doctoral Program of Higher Education and the National Nature Science Foundation of China (grant no. 20123221110013, 51173075 and 21271103) for financial support.

References

1. (a) S.–i. Noro, T. Ohba, K. Fukuhara, Y. Takahashi, T. Akutagawa and T. Nakamura, *Dalton Trans.*, 2011, **40**, 2268; (b) N. L. Rosi, J. Eckert, M. Eddaoudi, D. T. Vodak, J. Kim, M. O'Keeffe and O. M. Yaghi, *Science,* 2003, **16**, 1127; (c) C. Wang, D. M. Liu and W. B. Lin, *J. Am. Chem. Soc.,* 2013, **135**, 13222.
2. (a) S.–i. Noro, T. Akutagawa and T. Nakamura, *Chem. Commun.*, 2010, **46**, 3134; (b) B. L. Chen, S. Q. Ma, E. J. Hurtado, E. B. Lobkovsky and H. C. Zhou, *Inorg. Chem.,* 2007, **46**, 8490.
3. A. Nalaparaju and J. W. Jiang, *J. Phys. Chem. C,* 2012, **116**, 6925.
4. (a) H. W. Hou, L. X. Xie, G. Li, T. Z. Ge, Y. T. Fan, Y. Zhu, *New. J. Chem.,* 2004, **28**, 191; (b) B. Xiao, H. W. Hou, Y. T. Fan, *J. Organomet Chem.* 2007, **692**, 2014; (c) P. Y. Wu, C. He, J. Wang, X. J. Peng, X. Z. Li, Y. L. An and C. Y. Duan, *J. Am. Chem. Soc.,* 2012, **134**, 14991; (d) D. B. Dang, P. Y. Wu, C. He, Z. Xie and C. Y. Duan, *J. Am. Chem. Soc.,* 2010, **132**, 14321.
5. (a) C. Dey, R. Das, B. K. Saha, P. Podda and R. Banerjee, *Chem. Commun.,* 2011, **47**, 11008; (b) M.–X. Hu, Y.–G. Chen, C.–J. Zhang and Q.–J. Kong, *CrystEngcomm,* 2010, **12**, 1454; (c) S. K. Langley, N. F. Chilton, B. Moubaraki and K. S. Murray, *Chem. Commun.,* 2013, **49**, 6965; (d) M. Kurmoo, *Chem. Soc. Rev.,* 2009, **38**, 1353.
6. (a) H. W. Hou, Y. L. Wei, Y. L. Song, L. W. Mi, M. S. Tang, L. K. Li and Y. T. Fan, *Angew. Chem., Int. Ed.* 2005, **44**, 6067; (b) H. Y. Han, Y. L. Song, H. W. Hou, Y. T. Fan and Y. Zhu, *Dalton Trans.*, 2006, 1972.
7. (a) X.–Y. Dong, R. Wang, J.–B. Li, S.–Q. Zang, H.–W. Hou and T. C. W. Mak, *Chem. Commun.*, 2013, **49**, 10590; (b) R. Wang, X. –Y. Dong, H. Xu, R. –B. Pei, M.–L. Ma, S.–Q. Zang, H.–W. Hou and T. C. W. Mak, *Chem. Commun.*, 2014, **50**, 9153.
8. (a) Z. C. Hu, S. Pramanik, K. Tan, C. Zheng, W. Liu, X. Zhang, Y. J. Chabal and J. Li, *Cryst. Growth Des.,* 2013, **13**, 4204; (b) Z. C. Hu, B. J. Deibert and J. Li, *Chem. Soc. Rev.,* 2014, **43**, 5815.
9. (a) P.–C. Guo, Z. Y. Chu, X.–M. Ren, W.–H. Ning,W. Q. Jin, *Dalton Trans.,* 2013, **42**, 6603; (b) K. Takahashi, N. Hoshino, T. Takeda, S.–i. Noro, T. Nakamura, S. Takeda and T. Akutagawa, *Dalton Trans.*, 2014, **43**, 9081.

10. (a) H. W. Hou, Y. L. Wei, Y. L. Song, Y. Zhu, L. K. Li, Y. T. Fan, *J. Mater. Chem.,* 2002, **12**, 838; (b) X. Jing, C. He, Y. Yang and C. Y. Duan, *J. Am. Chem. Soc.,* 2015, **137**, 3967.
11. (a) Z. Lu, H. Xing, R. Sun, J. Bai, B. Zheng, Y. Li, *Cryst. Growth Des.* 2012, **12** 1081; (b) P. M. Schoenecker, C. G. Carson, H. Jasuja, C. J. J. Flemming, K. S. Walton, *Ind. Eng. Chem. Res.* 2012, **51**, 6513.
12. (a) T. J. Wu, L. J. Shen, M. Luebbers, C. Hu, Q. M. Chen, Z. Ni and R. I. Masel, *Chem. Commun.*, 2010, **46**, 6120; (b) J. G. Nguyen and S. M. Cohen, *J. Am. Chem. Soc.,* 2010, **132**, 4560; (c) J. Yang, A. Grzech, F. M. Mulder and T. J. Dingemans, *Chem. Commun.,* 2011, **47**, 5244.
13. (a) Y. Fu, G. Li, F. Liao, M. Xiong and J. Lin, *J. Mol. Struct.,* 2011, **1004**, 252; (b) C.–Y. Sun, S.–X. Liu, D.–D. Liang, K.–Z. Shao, Y.–H. Ren, and Z.–M. Su, *J. Am. Chem. Soc.,* 2009, **131**, 1883.
14. X. Chen, A. M. Plonka, D. Banerjee, J. B. Parise, *Cryst. Growth Des.,* 2013, **13**, 326.
15. (a) M. Dincă, W. S. Han, Y. Liu, A. Dailly, C. M. Brown and J. R. Long, *Angew. Chem., Int. Ed.,* 2007, **46**, 1419; (b) M. Dincă and J. R. Long, *J. Am. Chem. Soc.,* 2007, **129**, 11172; (c) M. Dincă, and J. R. Long, *J. Am. Chem. Soc.,* 2005, **127**, 9376.
16. Bruker, APEX 2, SAINT, XPREP, Bruker AXS Inc., Madison, Wisconsin, USA, 2007.
17. Bruker, SADABS, Bruker AXS Inc., Madison, Wisconsin, USA, 2001.
18. G. M. Sheldrick, SHELXS97 and SHELXL97: Program for the refinement of crystal structure, University of Göttingen, Germany, 1997.
19. P. J. Calderonea, D. Banerjeea, A. M. Plonkab, S. J. Kimc, J. B. Parise, *Inorg. Chim. Acta.,* 2013, **394**, 452.
20. Y. Y. Mao, J. W. Li, W. Cao,Y. L. Ying, L. W. Sun, and X. S. Pen, *Appl. Mater. Interfaces,* 2014, **6**, 4473.
21. (a) W. Chen, J. Y. Wang, C. Chen, Q. Yue, H. M. Yuan, J. S. Chen and S. N. Wang, *Inorg. Chem.,* 2003, **42**, 944; (b) Y.–Q. Sun, J. Zhang, Y.–M. Chen and G.–Y. Yang, *Angew. Chem., Int. Ed.,* 2005, **44**, 5814.

22. Z.–F. Wu, B. Tan, J.–Y. Wang, C.–F. Du, Z.–H. Deng and X.–Y. Huang, *Chem. Commun.,* 2015, **51**, 157.
23. (a) Q. F. Zhang, H. G. Hao, H. N. Zhang, S. N. Wang, J. Jin, D. Z. Sun, *Eur. J. Inorg. Chem.* 2013, 1123; (b) X. Zhang, Y. Y. Huang, J. K. Cheng, Y. G. Yao, J. Zhang, F. Wang, *CrystEngComm,* 2012, **14**, 4843.

The composites of **1** with hydrophobic PVDF were prepared by mechanically mixed, tableted and annealed approach, which showed good compatibility between **1** and PVDF, high hydrostability and intense blue emission.